Helsinki Institute of Physics

HIP-2001-06
November 15, 2001

Observation of K^0_S Decays in the NOMAD Silicon TARget (STAR) Detector

J. Kokkonen

Helsinki Institute of Physics[1] & CERN[2]

Abstract

The performance of the STAR detector, installed in the NOMAD short-baseline neutrino experiment at CERN, was investigated through an analysis of K^0_S-particles. This involved selecting a sample of K^0_S-particles both produced and decaying in STAR, including decays very close to the primary vertex. The sample was then used to obtain the vertex and double vertex resolutions of the detector.

[1]Helsinki Institute of Physics, P.O. Box 64, FIN-00014 University of Helsinki, Finland
[2]CERN, CH-1211 Geneva 23, Switzerland

1 Introduction

The NOMAD Silicon TARGet (STAR) was installed in the NOMAD short baseline neutrino experiment [1] at the CERN Super Proton Synchrotron for the 1997 and 1998 neutrino runs. STAR is placed within the NOMAD magnet in front of the drift chambers, as shown in Fig. 1.

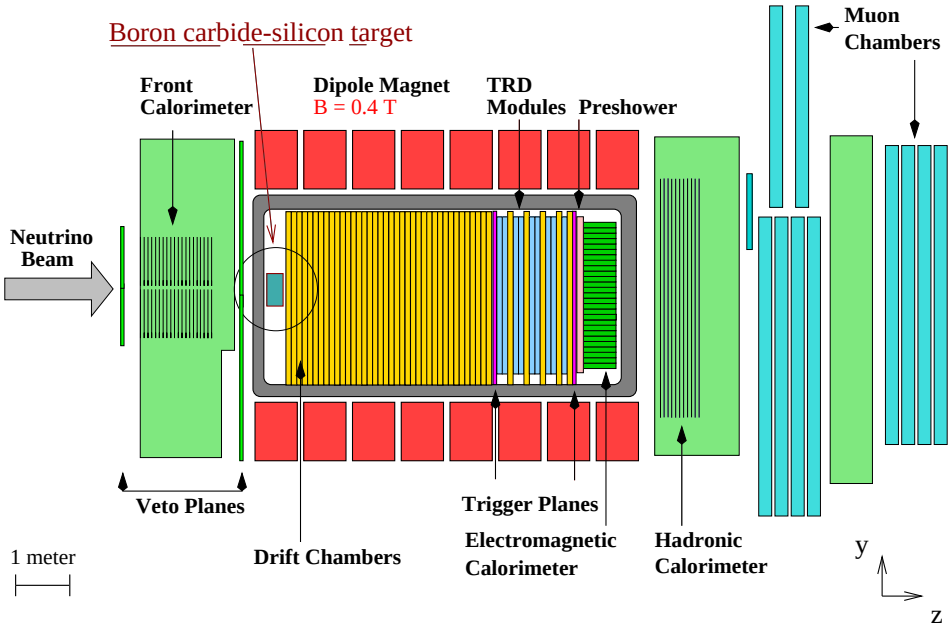

Figure 1: A sideview of the NOMAD detector, including STAR.

STAR was constructed principally to determine whether such a detector could be used for a future $\nu_\mu \leftrightarrow \nu_\tau$ oscillation experiment. The tau-particle resulting from a ν_τ charged current interaction would be identified using vertex criteria, while NOMAD, for example, uses kinematic criteria. The high precision of silicon technology would allow determining the positions of the primary neutrino interaction vertex and the secondary decay vertex in the case of a multi-prong tau-decay. For single-prong tau decays, the impact parameter could be measured.

STAR consists of five layers of silicon microstrip detectors perpendicular to the beam. The silicon layers are separated by 3.6 cm and have dimensions of 72 cm horizontally and 32 cm vertically, with a total area of 1.14 m^2. The strips are oriented horizontally with a readout pitch for the strips of 50 μm. The total number of readout strips is 32000. The five silicon layers are interleaved with four layers of 2.0 cm thick boron-carbide target (B_4C). A B_4C layer is positioned in front of each of the first four silicon layers with the fifth layer of silicon serving to improve the tracking. The total mass of the target is 45 kg, with a depth of 0.37 radiation lengths and 0.25 interaction lengths. If the material due to the five silicon planes is included, there are a further 0.18 radiation lengths on average and 0.23 at maximum, depending on the path followed within the detector. STAR is shown in Fig. 2 and a detailed description can be found in [2].

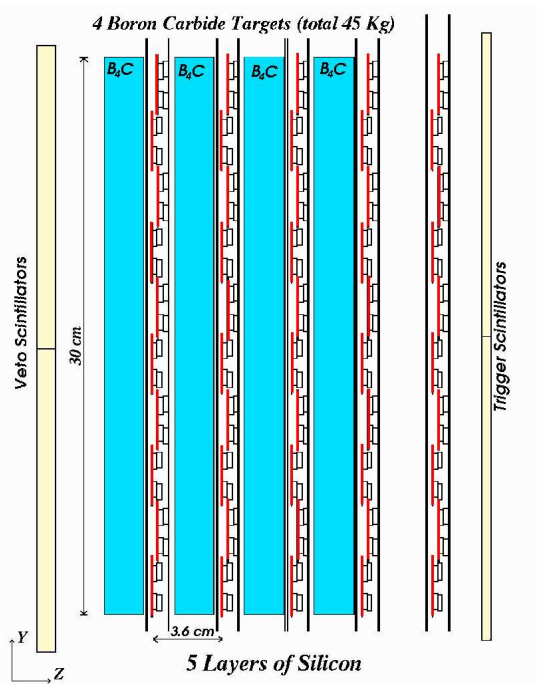

Figure 2: A sideview of the NOMAD-STAR silicon detector.

The aim of this study is to obtain the vertex and double vertex resolutions of STAR by observing K^0_S-particles. This, along with the impact parameter resolution, would allow one to evaluate the performance of a STAR-like detector in a search for short-lived particles. The present work gives indications, for example, of the efficiency to detect decays in the $\tau \to 3\pi$ channel in a $\nu_\mu \leftrightarrow \nu_\tau$ oscillation experiment. Other studies of the data in STAR include charm decays [3] and further studies could include more exotic topics such as a search for short-lived neutral heavy leptons.

This memo is organised as follows. Section 2 gives a brief overview of the track and vertex reconstruction. Section 3 discusses both the simulated and experimental data samples and gives some basic definitions related to the analysis. In Section 4, the selection cuts on the various parameters that are used to obtain a sample of K^0_S-particles are presented. Section 5 describes the resulting K^0_S-sample and some of its properties. The various vertex resolutions are obtained in Section 6. Finally, the conclusions are presented.

2 STAR reconstruction

2.1 Reconstruction and simulation packages

The STAR reconstruction sofware is compiled out of various NOMAD software packages that have been extensively modified to incorporate STAR. The beam for the Monte Carlo data was simu-

lated using NUBEAM 4.00 and Gfluka/fluka 92. The events are generated using NEGLIB 5.090. The detector was simulated using a modified version of GENOM 5.1213, which includes a detailed description of STAR.

2.2 Event reconstruction in STAR

The configuration of STAR results in some important differences in event reconstruction with respect to the NOMAD drift chambers (DC). Primarily, the silicon offers excellent position resolution. However, it can only measure in two dimensions, namely in the yz-plane, and tracks are built out of hits from a maximum of five layers. Further difficulties are introduced by multiple scattering and by other interactions occuring in the large amount of material traversed by each particle. Finally, the small mass of STAR results in far fewer neutrino interactions than in the drift chambers.

The position of each hit is calculated using a charge-sharing model described in detail in [4]. The hits are assigned to tracks in STAR by extrapolating a DC track backwards into STAR. The DC track is required to have a reconstructed momentum of at least 150 MeV/c. Hits within a certain roadwidth, which depends on the track momentum, are selected for the track. A STAR track is built if there are at least two hits along the path of the track and at most one silicon plane not containing a hit (a gap). However, further gaps are allowed if a track passes through or close to inactive areas in the detector. Each hit can be attached to only one track. Apart from using the total momentum provided by the DC, the STAR track is reconstructed using only the assigned STAR hits. A Kalman filtering technique is used to account for multiple scattering. This is described in detail in [5]. Further information on the STAR track can be obtained from its corresponding DC track, including its approximate x-position and particle identification.

When the STAR tracks have been reconstructed, a primary vertex is built. For neutrino runs (as opposed to anti-neutrino runs), the highest momentum negative muon is selected as the seed track. If there are none, the highest momentum negative track is used. If there are no negative tracks at all, the highest momentum positive track is used. The procedure for anti-neutrino runs is the same except that tracks of the opposite charge are considered. Next, the crossing points of the seed track and the other tracks are found. The impact parameters of all the other tracks relative to each of these vertex position estimates are then found. The combination of tracks that gives the highest number of tracks within 250 μm is used to build the primary vertex. The position of the primary vertex is determined using a Kalman filtering technique [5].

3 Experimental and simulated data samples

3.1 Defining K^0_S decay candidates

Searches in STAR are limited to short-lived particles as the particles have to be produced and decay within STAR. In the z-direction, the fiducial volume spans from the first B_4C layer up to

the fourth silicon layer (as hits in at least two planes are required for track-building, interactions occuring after the fourth silicon plane cannot be used). The fiducial volume is then defined as:

- -35.9 $cm \leq x \leq$ 36.3 cm
- -38.9 $cm \leq y \leq$ -7.3 cm
- 6.0 $cm \leq z \leq$ 19.7 cm

K^0_S particles are searched for through their decay to $\pi^+\pi^-$, for which the branching ratio is (68.68 $\pm$ 0.28)%. In addition, there are $\pi^0\pi^0$ decays with a branching ratio of (31.39 $\pm$ 0.28)% as well as some rarely occuring decays [6]. The Monte Carlo (MC) only simulates the $\pi^+\pi^-$ and $\pi^0\pi^0$ decays [7].

In the Monte Carlo sample, tracks reconstructed in the DC are matched to generated tracks. By finding which reconstructed DC track a STAR track is matched to, the correspondence between reconstructed STAR tracks and generated Monte Carlo tracks is established.

The present analysis only uses tracks reconstructed by STAR. Furthermore, only those STAR tracks which are not attached to the primary vertex, i.e. free tracks, are considered as potential K^0_S decay products. Every pairing of a positive and negative free track is considered as a potential K^0_S decay candidate and is termed a track pair.

A free track originating from a K^0_S decay is defined as a signal track, while all other free tracks are background tracks. A track pair is defined as signal if both the tracks originate from the same K^0_S. The combinations of a signal track and a background track, or even two signal tracks from different K^0_S, form a background pair.

Only events containing a reconstructed primary vertex (with at least two reconstructed STAR tracks) and at least one free positive and one free negative reconstructed STAR track can yield reconstructed K^0_S-particles. These events are refered to as "2+1+1"-events even if there are more than the minimum required number of tracks in the primary vertex or more than the minimum required number of free tracks.

3.2 The Monte Carlo and experimental data samples

The Monte Carlo sample consists of 68955 ν_μ charged-current (CC) and 19837 ν_μ neutral-current (NC) events occuring within the fiducial volume of STAR. As the ratio of neutral-current events to charged-current events is 0.312 [6], a normalization factor of 0.901 is used for the charged-current sample to combine the samples. This gives 81965 events in the combined MC sample. This assumes that the reconstruction efficiency is the same for both charged-current and neutral-current events. The predicted flux of the neutrino beam in STAR consists of 94.1 % ν_μ, 5.0 % $\overline{\nu}_\mu$, 0.7 % ν_e and 0.2 % $\overline{\nu}_e$ [3]. Therefore the effects of electron-neutrinos and anti-neutrinos of all flavours in the beam was considered negligible for this study and were not included in the sample. Likewise,

quasi-elastic events were not simulated, given their low probability of generating events of the "2+1+1"-configuration.

A potential problem was uncovered with the Monte Carlo sample at the simulation level, most likely due to a misinterpretation of the Monte Carlo databank information. In approximately 10% of events containing a K^0_S decay vertex, the types or numbers of the K^0_S daughter particles was incorrect. These events were discarded. In a small number of cases, events were also discarded due to an unacceptably high multiplicity of generated particles or of reconstructed STAR tracks.

The experimental data sample consisted of the entire 1998 data set of 11527 filtered events. Of these, 10942 contained a reconstructed STAR primary vertex, compared to 71698 in the combined MC sample. This gives 0.153 as the ratio of experimental data events to MC events. Looking at the "2+1+1"-events, the experimental data sample contains 2604 and the combined MC sample 24096 events, giving a ratio of 0.108.

The details of the event selection are shown in Table 1. Also shown are the total number of free positive and free negative tracks as well as track pairs for the "2+1+1"-events. For the Monte Carlo sample, these are split into signal and background. The analysis of the Monte Carlo sample is performed for a large part separately for signal and background pairs.

Selection criterion	$\nu_\mu CC$ MC	$\nu_\mu NC$ MC	Combined MC	Data	Data:MC
Total events	68955	19837	81965	11527	0.141
No anomalous decays	67897	19544	80719	-	-
Acceptable multiplicity	67841	19534	80659	11526	0.143
Reconstructed primary	62385	15489	71698	10942	0.153
"2+1+1"	21295	4909	24096	2604	0.108
Total +/- free tracks	42129/34263	9943/7615	47901/38486	4592/3696	0.096/0.096
+/- signal tracks	686/754	146/127	764/806	-	-
+/- background tracks	41443/33509	9797/7488	47137/37680	-	-
Total track pairs	71069	16147	80180	6714	0.084
Signal track pairs	324	50	342	-	-
Background track pairs	70745	16097	79838	-	-

Table 1: The simulated and experimental data samples.

The 47901 positive and 38486 negative free tracks in the combined Monte Carlo sample give an average free track multiplicity of 3.6 per event. The corresponding figures for the experimental data are 4592 positive and 3696 negative free tracks and an average free track multiplicity of 3.2. The free track multiplicities are shown in Fig. 3, for which the normalization is done by the number of events. Furthermore, the Monte Carlo sample contains 3.3 track pairs per event, while the experimental sample only contains 2.6. This points to differences in track reconstruction efficiencies between the Monte Carlo simulation and experimental data.

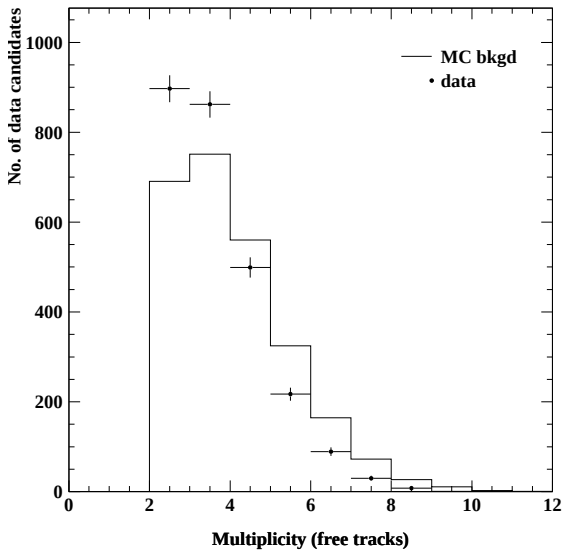

Figure 3: Comparison of free track multiplicities in the Monte Carlo and the experimental data.

It is also interesting to note that for both the Monte Carlo and experimental data samples, there are approximately 20% less free negative tracks than positive tracks. This simply reflects the ratio of positive to negative tracks in the hadron shower.

Finally, an estimate for the number of reconstructable K^0_S-particles in the experimental data can be made using the MC sample. There are 342 signal track pairs in the combined sample. If one uses the number of events with a reconstructed primary vertex as the basis for normalization, one would expect 52 ± 3 reconstructable K^0_S decays before application of selection cuts in the experimental data. The error is based on the statistical error of the MC sample. Using the "2+1+1"-events gives 37 ± 2 reconstructable K^0_S decays. If the anomalous decays are assumed to be legitimate decays which have been misinterpreted, the number of reconstructable K^0_S decays increases by 10%.

3.3 Reconstruction efficiency before cuts

The reconstruction efficiency of K^0_S-particles is calculated before the application of selection cuts. The combined $\nu_\mu CC$ and $\nu_\mu NC$ Monte Carlo sample, after removing the events with the anomalous decays and high particle or track multiplicities, is used. Only decays to charged pions that occur within the STAR fiducial volume, defined in Section 3.1, are considered.

Of the 8503 K^0_S-particles decaying to charged pions, only 2241 do so within the STAR fiducial volume, as shown in Table 2. The efficiency is calculated relative to this number as only these decays are detectable by STAR. Of the resulting decay tracks, 57% are reconstructed by the drift chambers. As shown by Fig. 4, the lost tracks mostly have a momentum below 0.8 GeV/c. These

results are not surprising as, on average, the particles traverse several centimeters of boron-carbide before reaching the drift chambers. Unfortunately, the loss of a DC track straight away implies the loss of a STAR track as STAR tracks are built using the DC tracks.

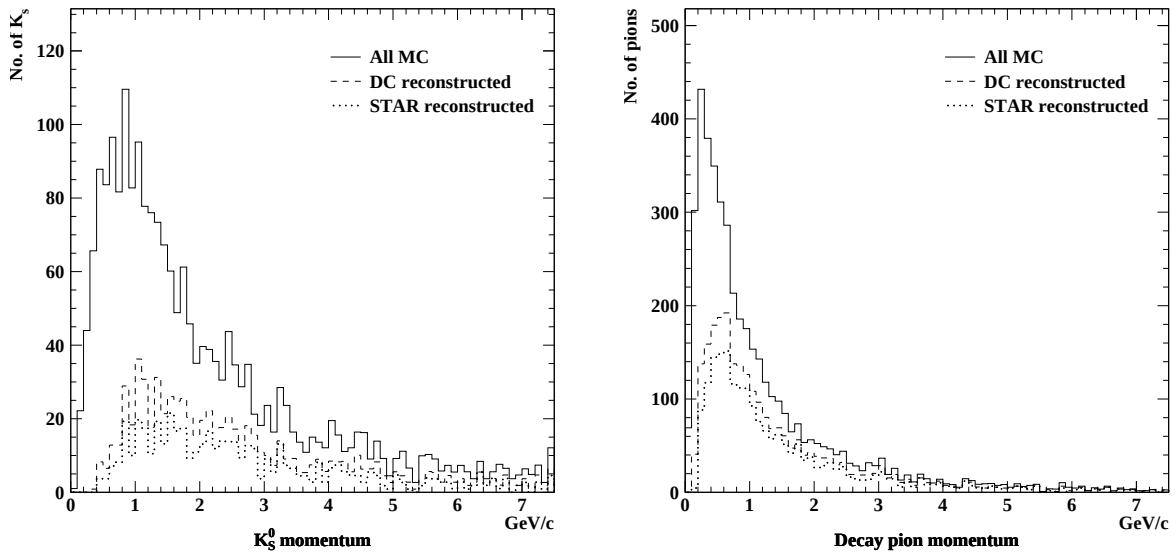

Figure 4: Momenta of the K^0_S and decay pions. The solid line corresponds to the full simulated MC sample, the dashed line to the particles reconstructed in DC and the dotted line to particles reconstructed in STAR.

Of all the reconstructed DC decay tracks, approximately 80% have corresponding STAR tracks. However, to reconstruct a K^0_S-vertex, both the positive and the negative decay pions have to be reconstructed. This requirement reduces the K^0_S sample to 547, giving a reconstruction efficiency of 24.4%. The sample is further reduced to 291 K^0_S-particles when both decay tracks are required to be free, i.e. not attached to the primary vertex. This finally gives a reconstruction efficiency of 13.0%.

As the reconstruction is done in the yz-plane, only information of the decay as a projection onto this plane is available. Therefore decays occuring in the horizontal plane or close to it would be indistinguishable from the hadron shower and a secondary vertex cannot be built. Furthermore, for events with low multiplicity, the K^0_S decay tracks can mistakenly be used to form the primary vertex, irrespective of the decay plane.

The requirement of free tracks brings out a difference between the charged-current and neutral-current Monte Carlo samples. They both have approximately the same efficiency for reconstructed STAR tracks, but for the neutral-current sample they are incorrectly attached to the primary vertex more often (51.7% of the time compared to 25.7% for the charged-current sample). This is even more pronounced for the negative decay pions, pointing to difficulties in reconstructing the primary vertex. The primary vertex algorithm has a bias in selecting negative tracks as the seed

track. The majority of runs are neutrino runs and for them, if no negative muon is found for the seed, the highest momentum negative track is taken. For anti-neutrino runs the algorithm is the same, except that positive tracks are selected.

Finally, it should be pointed out that although the normalized Monte Carlo sample has 291 fully reconstructed K^0_S-particles, a further 51 decays are reconstructed when the requirement of the decay fiducial volume is lifted on the generated K^0_S position (there were 342 reconstructed decays obtained in the previous section). This was found to be due to hits being incorrectly attached to some tracks. This resulted in the reconstruction of decays actually occuring outside the fiducial volume to be incorrectly reconstructed within the fiducial volume. The above results are summarized in Table 2.

Selection criterion	$\nu_\mu CC$ MC	$\nu_\mu NC$ MC	Combined MC	Efficiency (%)
Total $K^0_S \to \pi^+\pi^-$	7196	2019	8503	-
Decay in fiducial volume	1884	544	2241	100.0
+/- DC tracks	1079/1097	314/308	1286/1296	57.4/57.8
+/- STAR tracks	855/880	262/245	1032/1038	46.1/46.3
Both STAR tracks	448	143	547	24.4
+/- free STAR tracks	654/635	150/95	739/667	33.0/29.8
Both STAR tracks free	277	41	291	13.0
STAR reconstructed K^0_S	324	50	342	-

Table 2: The Monte Carlo reconstruction efficiency.

4 Selection cuts for K^0_S-particles

The individual selection cuts for the experimental data are discussed in this section. A two-fold approach is taken. Firstly, it is important to see how good the agreement between the simulated and experimental data is. The simulated background before any selection cuts for the different variables used for the cuts themselves are compared with the full experimental data sample by normalizing the distributions using the number of track pairs. Although the experimental data sample also contains signal, for most distributions before application of selection cuts it is overwhelmed by the background. This comparison is done to show that the agreement between experimental and simulated data is, in general, very good. Secondly, the Monte Carlo signal and background are compared so that an appropriate value for a selection cut can be chosen. This is always done for the surviving combinations or tracks, i.e. for those cases which have passed the cuts introduced up to that point.

The plots on the variables in this section are shown with the comparison of experimental data to simulated data *before* cuts on the left-hand side. On the right-hand side, the simulated background and simulated signal are compared for *surviving* combinations. The signal has been scaled such that the highest bins for signal and background are equally high. Some plots are shown for the

regions around the cut and not for the full distribution.

It should be noted that most of the selection cuts do not depend strongly on the kind of V^0 that is searched for (a V^0 is a neutral particle decaying into two charged particles). The initial cuts are general with the last cuts specifically selecting a K^0_S decay. The results are summarized in the tables in Section 4.12. Table 3 contains the results for the Monte Carlo simulated signal and Table 4 those for the Monte Carlo background. Table 5 gives the results for the data.

4.1 Fully reconstructable track pairs

For signal decay tracks, there should be no hits upstream of the crossing point of the track pair. However, tracks are sometimes misreconstructed using hits actually belonging to other tracks (or using hits due to noise) in the vicinity of the primary vertex. Therefore the tracks in a combination are reconstructed again using only hits downstream of the crossing point. This is done separately for every pairing of tracks. These are referred to as fully reconstructable tracks. This means that the same track, depending on which other track it is paired with, could be reconstructed with a different number of hits. A further implication is that some decay track candidates are no longer reconstructed since tracks require at least two hits to be reconstructed. It should also be noted that this procedure results in no candidates being reconstructed downstream of the STAR fiducial volume and is therefore a *de facto* fiducial volume cut as well. The effect of the requirement of reconstructable track pairs on signal tracks is to remove false information due to the incorrect hits. Removing hits which are correctly assigned simply results in a slightly less accurate track as not all the information is used.

4.2 Secondary vertex position

An obvious requirement is that the decay occurs downstream of the primary interaction point. Fig. 5 shows the distance d_z between the primary vertex and secondary vertex candidate, with positive values indicating a downstream secondary vertex candidate. The simulated and experimental data agree very well in this variable and a cut of $d_z \geq 0.0\ cm$ has been chosen.

4.3 Pointing of K^0_S-candidate

An important variable is that of the pointing. This is defined as the difference in direction, Θ, between the momentum vector formed by the candidate pair and the direction-of-flight vector between the primary vertex and secondary vertex candidate. As the reconstruction is done in two dimensions, the vectors are in fact projections into the yz-plane. From Fig. 6, a cut of -0.12 $rad \leq \Theta \leq 0.12\ rad$ is chosen.

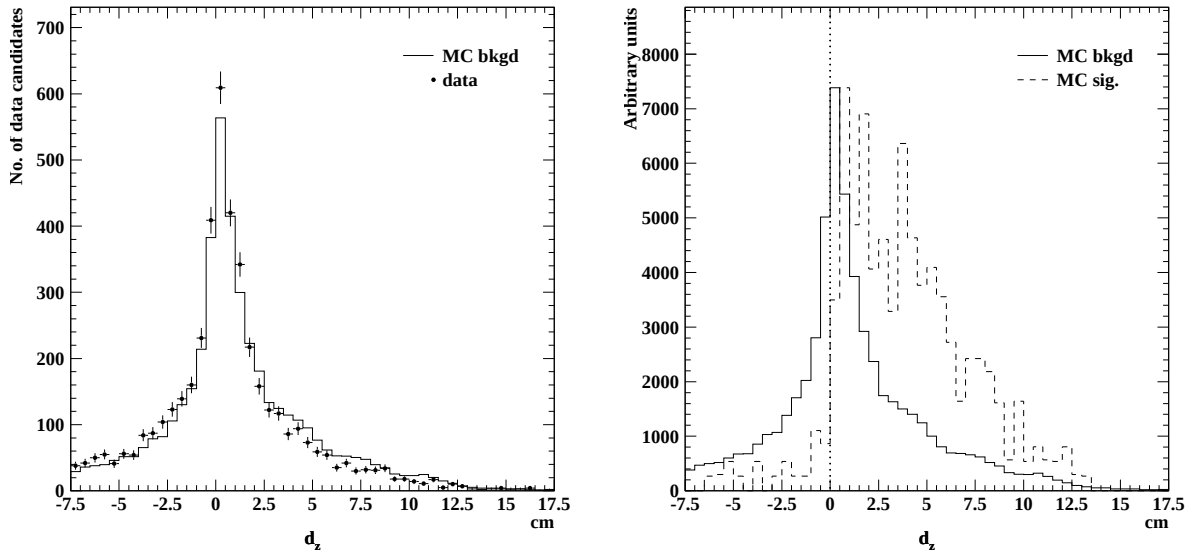

Figure 5: The distance d_z between the primary vertex and secondary vertex candidate. The experimental data is compared to Monte Carlo background before cuts on the left. The distributions of the simulated signal and background for surviving combinations is shown on the right. The vertical dotted line shows the position of the cut.

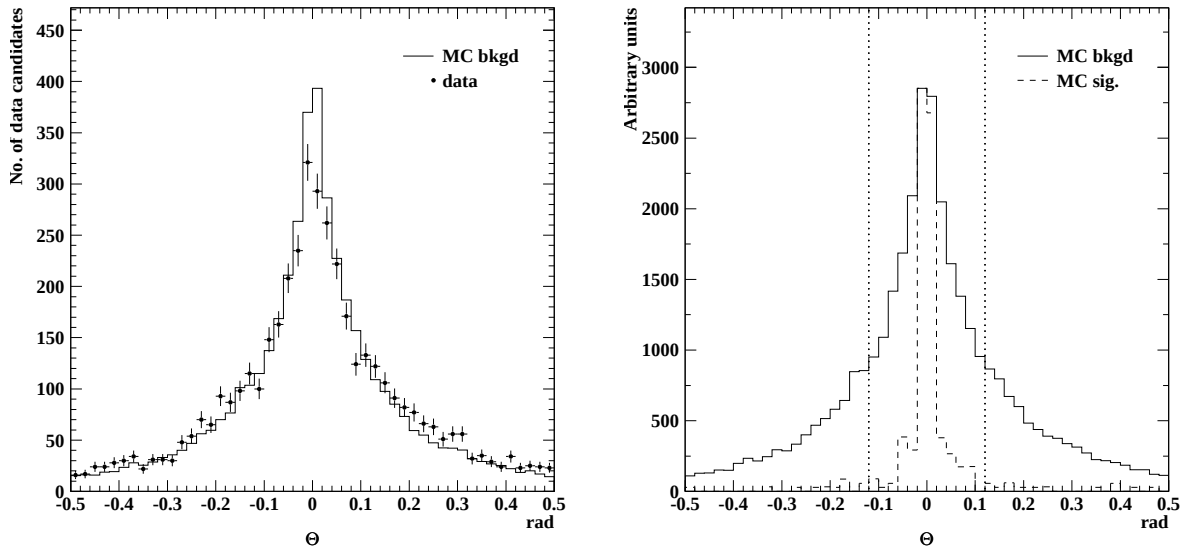

Figure 6: The direction of the momentum vector formed by the candidate pair with respect to the direction-of-flight vector. The experimental data is compared to Monte Carlo background before cuts on the left. The distributions of the simulated signal and background for surviving combinations is shown on the right. The vertical dotted lines show the positions of the cuts.

4.4 Track impact parameters

A significant source of background comes from tracks originating from the primary interaction. The impact parameter, $i.p.$, is defined as the closest signed distance of a track or its extrapolation to the primary vertex. The background is characterized by tracks having small impact parameters. Initially these tracks have not been included in the primary vertex as their impact parameters have been too large, but upon being reconstructed again using only downstream hits (fully reconstructable tracks), the positions and therefore impact parameters of the tracks may have changed. The track impact parameters can be seen in Fig. 7. As the reconstruction is done in only two dimensions, K^0_S decays in or close to the transverse plane become indistinguishable from the background. Thus there is also a small contribution to the small $i.p.$ region from signal events as well. The simulated data and experimental data agree very well. A cut is applied at $\mid i.p. \mid \geq 300\ \mu m$.

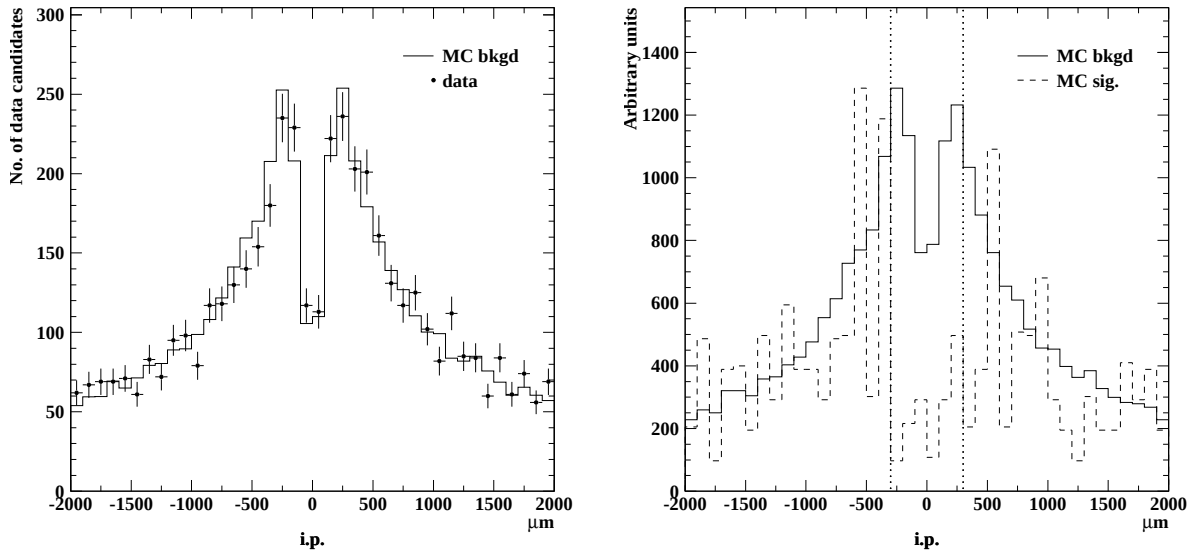

Figure 7: The signed impact parameter with respect to the primary vertex for individual tracks. The experimental data is compared to Monte Carlo background before cuts on the left. The distributions of the simulated signal and background for surviving combinations is shown on the right. The vertical dotted lines show the positions of the cuts.

4.5 Relative x-positions of track pairs

Although the x-coordinate is not used as such in the reconstruction (except for the momentum), some x-position information can be obtained from the DC track to which the STAR track is matched. The x-resolution of the DC is poor compared to the y- and z-resolutions. The resolution is further decreased when extrapolating the x-information of the DC track to STAR due to a lever-arm effect and multiple scattering. However, as a quality cut, it was required that the difference in x-position, Δx, of the two decay track candidate pairs at their intersection point in the yz-plane

be less than 1.0 cm. This choice of cut can be justified from the distributions in Fig. 8. It should also be noted that the simulated and experimental data agree very well.

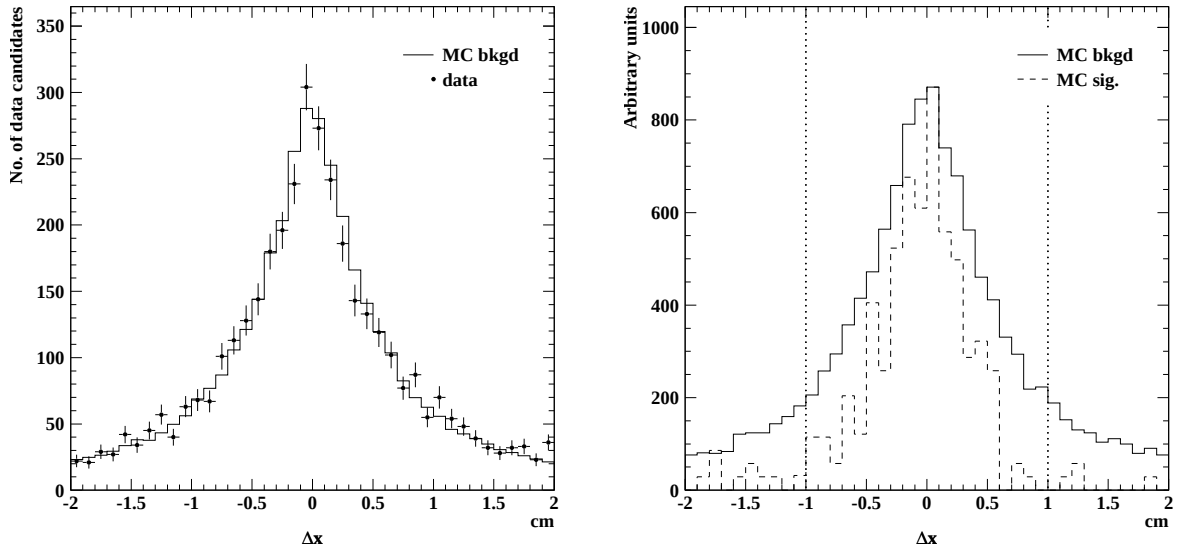

Figure 8: The difference in x-position of the candidate decay tracks at their intersection point in the yz-plane. The experimental data is compared to Monte Carlo background before cuts on the left. The distributions of the simulated signal and background for surviving combinations is shown on the right. The vertical dotted lines show the positions of the cuts.

4.6 Momentum of K^0_S-candidate

A cut is made on the total momentum of the K^0_S-candidate, as calculated from the momentum vectors of the two decay candidates, to prevent low-momentum and possibly poorly reconstructed candidates from being considered. Based on Fig. 9, the momentum of a decay candidate is required to be at least 0.8 GeV/c. There are some small discrepancies between the simulated and experimental data at low momenta.

4.7 Momentum asymmetry of track pairs

Fig. 10 shows the momentum ratio distributions for the higher momentum track to the lower momentum track in a combination. Occasionally, a particularly high-momentum track is paired with a low-momentum track. For the Monte Carlo simulated signal the momentum ratio of these tracks does not exceed 10. The agreement between simulated and experimental data is excellent. A cut of $0.1 \leq p_+/p_- \leq 10$ was chosen, where p_+ and p_- are the positive and negative track momenta, respectively. This serves as a quality cut.

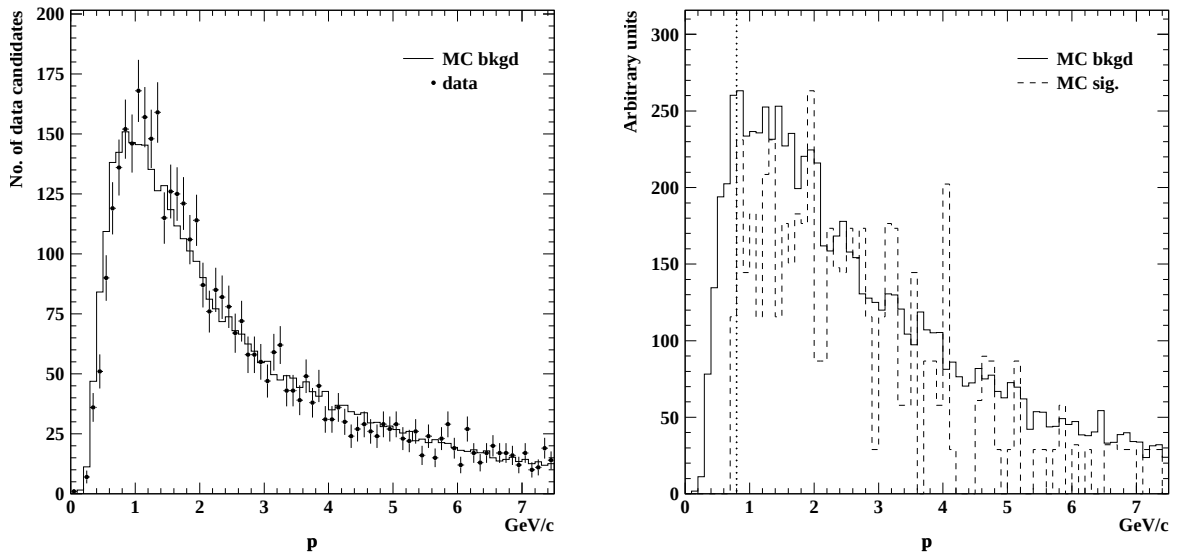

Figure 9: The total momentum of the candidate track pairs. The experimental data is compared to Monte Carlo background before cuts on the left. The distributions of the simulated signal and background for surviving combinations is shown on the right. The vertical dotted line shows the position of the cut.

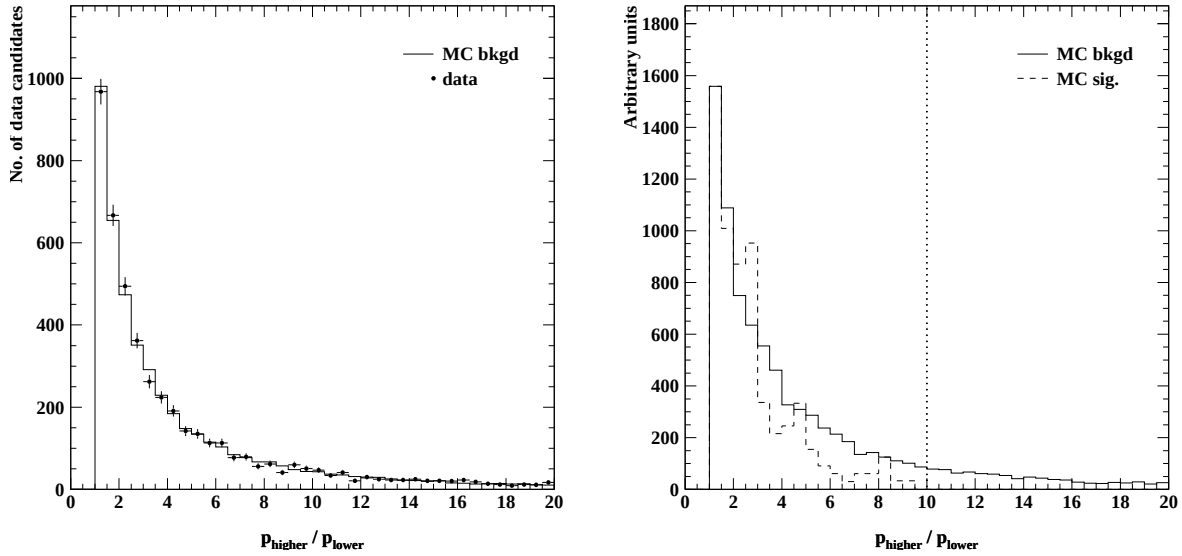

Figure 10: The momentum ratio of the track with the higher momentum, p_{higher}, to the track with the lower momentum, p_{lower}. The experimental data is compared to Monte Carlo background before cuts on the left. The distributions of the simulated signal and background for surviving combinations is shown on the right. The vertical dotted line shows the position of the cut.

4.8 Track χ^2 probability

A further quality cut is applied on the chi-squared probability of the DC tracks matched to the STAR tracks. The chi-squared of the DC track, instead of the corresponding STAR track, is used as it has far more hits. The χ^2 probability was required to be greater than or equal to 0.001 to eliminate poorly reconstructed tracks. Fig. 11 shows the distributions.

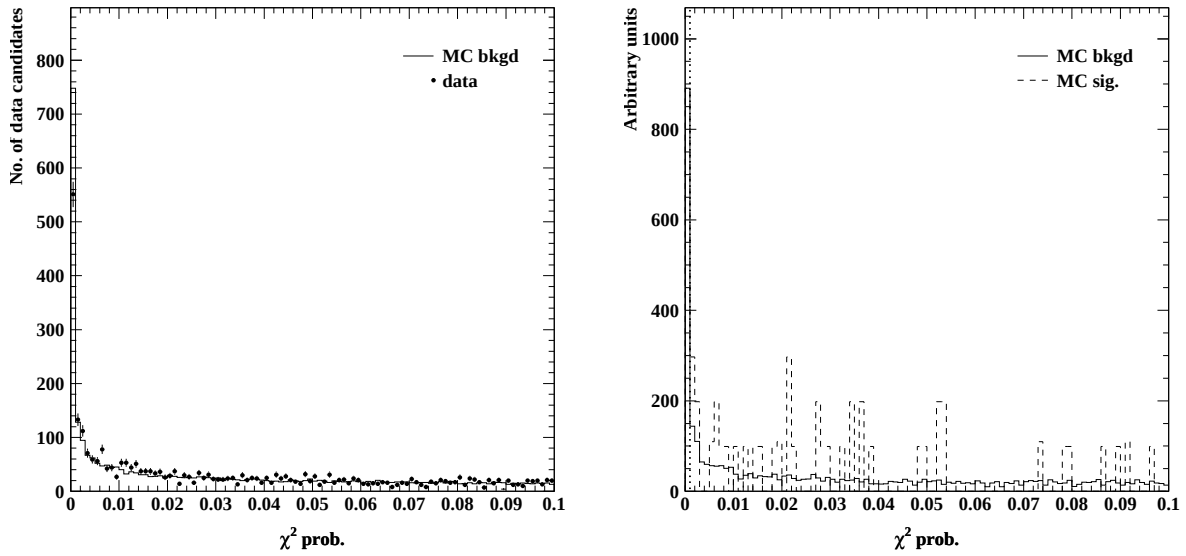

Figure 11: The chi-squared probability of the DC tracks matched to STAR tracks, with the low chi-squared probability region shown. The experimental data is compared to Monte Carlo background before cuts on the left. The distributions of the simulated signal and background for surviving combinations is shown on the right. The vertical dotted line shows the position of the cut.

4.9 Particle identification

The variables and cuts considered so far could be used for a general V^0 search. The momentum and momentum asymmetry cuts introduced earlier serve primarily as quality cuts, although they could affect the efficiency of some V^0 searches. The remaining cuts of particle identification, transverse momentum and lifetime cuts select a K^0_S decay.

STAR itself has no means of identifying the candidate decay particles, but the other sub-detectors in NOMAD can provide some information. In particular the muon identification is good. The identified muons, as well as identified electrons and positrons, are eliminated. Fig. 12 shows the particle identification of the tracks. Here "0" corresponds to unidentified particles, "3" to electrons and positrons, "5" to positive muons, "6" to negative muons, "8" to positive hadrons and "9" to negative hadrons.

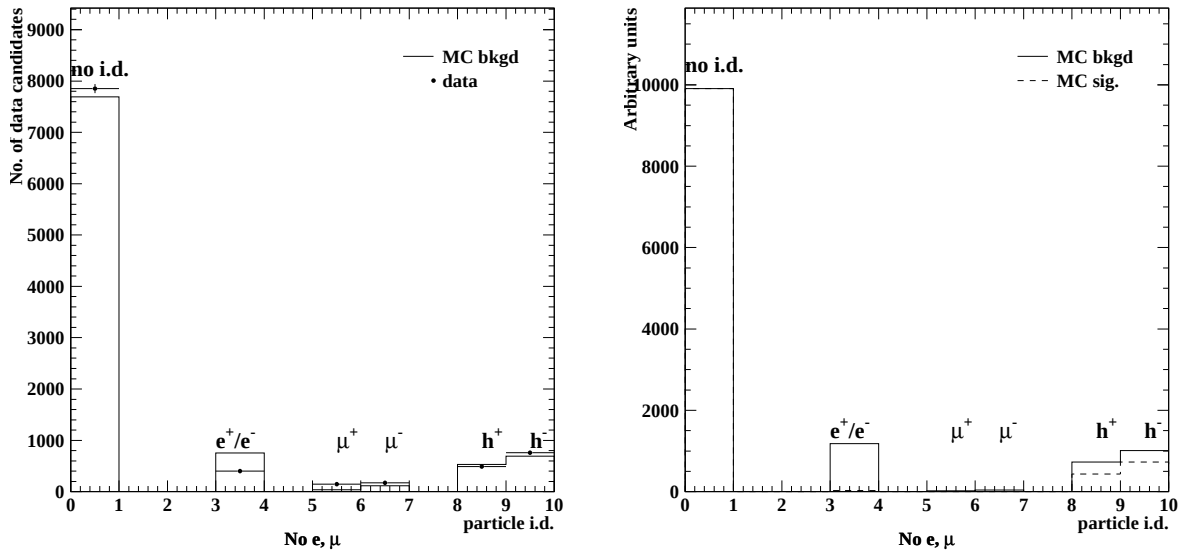

Figure 12: The particle identification of the candidate decay tracks. Hadrons are denoted by an "h". The experimental data is compared to Monte Carlo background before cuts on the left. The distributions of the simulated signal and background for surviving combinations is shown on the right.

4.10 Transverse momenta of decay candidates

The internal transverse momentum of the positive track with respect to the total momentum vector of the track pair is one of the most effective cuts, eliminating over half of the remaining background. A K^0_S decay is kinematically restricted to an internal transverse momentum of less than 0.206 GeV/c. Based on Fig. 13, a cut of 0.05 $GeV/c \leq\ p^+_T\ \leq 0.22\ GeV/c$ has been chosen. This cut also removes possible background due to gamma conversions. There is a discrepancy between the simulated and experimental data for low internal transverse momentum. This is due to the reconstruction efficiency of the experimental data being lower than that of the Monte Carlo sample for low-momentum tracks and small opening angle track pairs.

4.11 K^0_S candidate $c\tau$

The final cut is related to the lifetime. Here the lifetime is expressed as a distance by multiplying it by the velocity of light. It is denoted by $c\tau$ and is 2.6786 cm for the K^0_S [6]. By taking the boost into account, the apparent decay distances of the K^0_S candidates can be expressed in terms of the $c\tau$. The distributions are shown in Fig. 14 and have been used to obtain the cut of $c\tau \geq 0.1\ cm$. It should be remembered that as STAR is very short ($< 14\ cm$) most K^0_S do not decay in STAR and are therefore not reconstructable in it. This greatly affects the shape of the $c\tau$-distributions.

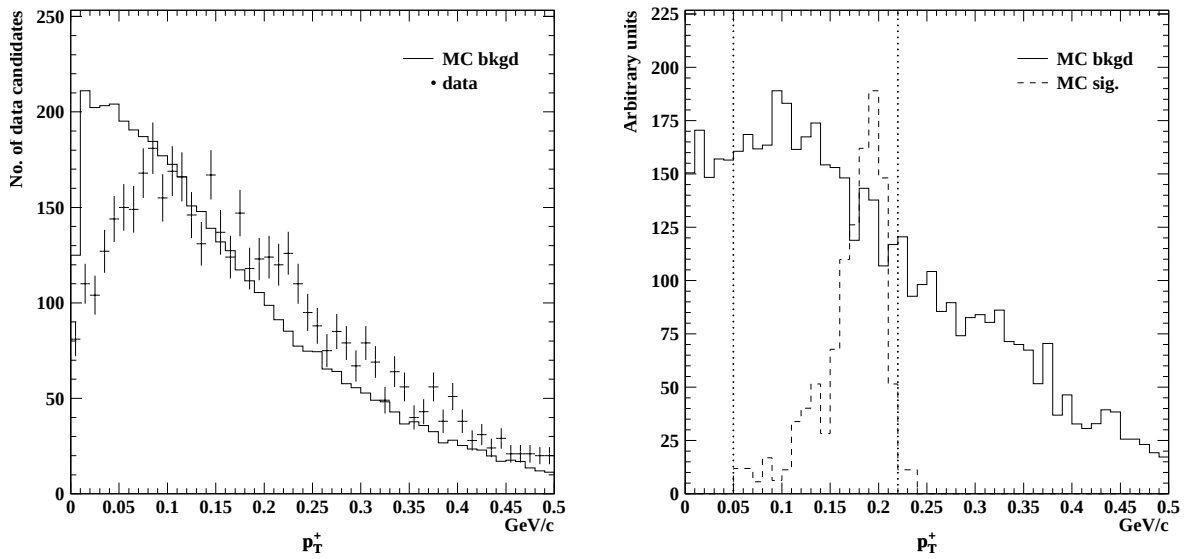

Figure 13: The interal transverse momentum of the candidate decay track pair. The experimental data is compared to Monte Carlo background before cuts on the left. The distributions of the simulated signal and background for surviving combinations is shown on the right. The vertical dotted lines show the positions of the cuts.

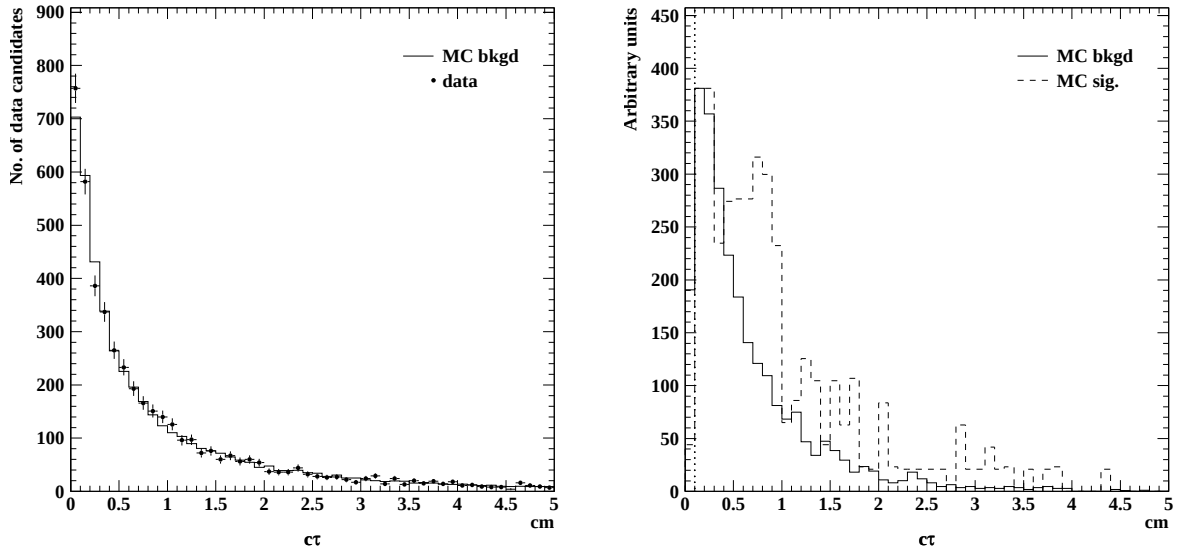

Figure 14: The $c\tau$ of the candidates under the K_S^0-hypothesis. The experimental data is compared to Monte Carlo background before cuts on the left. The distributions of the simulated signal and background for surviving combinations is shown on the right. The vertical dotted line shows the position of the cut.

4.12 Summary of cuts

The cuts are summarized in this section in tabular form. Table 3 shows the cut-by-cut breakdown for the Monte Carlo signal and Table 4 for the background. For the reconstructable K_S^0 decays, 49.4% are retained. Apart from the full reconstructability requirement and Δx cut, the relative efficiency of every cut is over 90%. After cuts, but with no requirement on the invariant mass, only 3.0% of the background remains. The effects of the cuts on the data is shown in Table 5. The cuts have a more severe effect on the experimental data, with only 2.1% of the sample despite it also containing signal.

Cut	$\nu_\mu CC$	$\nu_\mu NC$	Combined	Eff. (%)	Rel. eff. (%)
"2+1+1"	324	50	342	100.0	100.0
Fully reconstructable	261	38	273	79.8	79.8
$d_z \geq 0.0\ cm$	245	34	255	74.6	93.4
-0.12 $rad \leq \Theta \leq 0.12\ rad$	222	30	230	67.3	90.2
$\mid i.p. \mid \geq 300\ \mu m$	212	26	217	63.5	94.3
-1.0 $cm \leq \Delta x \leq 1.0\ cm$	180	25	187	54.7	86.2
$p \geq 0.8\ GeV/c$	176	25	184	53.8	98.4
$0.1 \leq p_+/p_- \leq 10$	176	25	184	53.8	100.0
χ^2 prob. ≥ 0.001	167	25	175	51.2	95.1
No e, μ	166	25	175	51.2	100.0
$0.05\ GeV/c \leq p_T^+ \leq 0.22\ GeV/c$	162	25	171	50.0	97.7
$c\tau \geq 0.1\ cm$	161	24	169	49.4	98.8

Table 3: The number of events passing the selection cuts for the Monte Carlo signal.

Cut	$\nu_\mu CC$	$\nu_\mu NC$	Normalized	Eff. (%)	Rel. eff. (%)
"2+1+1"	70745	16097	79838	100.0	100.0
Fully reconstructable	56051	12815	63317	79.3	79.3
$d_z \geq 0.0\ cm$	34532	6485	37598	47.1	59.4
-0.12 $rad \leq \Theta \leq 0.12\ rad$	18564	3305	20031	25.1	53.3
$\mid i.p. \mid \geq 300\ \mu m$	13200	2449	14342	18.0	71.6
-1.0 $cm \leq \Delta x \leq 1.0\ cm$	8830	1695	9651	12.1	67.3
$p \geq 0.8\ GeV/c$	8034	1530	8769	11.0	90.9
$0.1 \leq p_+/p_- \leq 10$	6780	1198	7307	9.2	83.3
χ^2 prob. ≥ 0.001	5979	1061	6448	8.1	88.2
No e, μ	4982	865	5354	6.7	83.0
$0.05\ GeV/c \leq p_T^+ \leq 0.22\ GeV/c$	2441	409	2608	3.3	48.7
$c\tau \geq 0.1\ cm$	2265	377	2418	3.0	92.7

Table 4: The number of events passing the selection cuts for the Monte Carlo background.

Cut	Data	Eff. (%)	Rel. eff. (%)
"2+1+1"	6714	100.0	100.0
Fully reconstructable	4910	73.1	73.1
$d_z \geq 0.0\ cm$	2695	40.1	54.9
-0.12 $rad \leq \Theta \leq 0.12\ rad$	1246	18.6	46.2
$\mid i.p. \mid \geq 300\ \mu m$	880	13.1	70.6
-1.0 $cm \leq \Delta x \leq 1.0\ cm$	557	8.3	63.3
$p \geq 0.8\ GeV/c$	518	7.7	93.0
$0.1 \leq p_+/p_- \leq 10$	432	6.4	83.4
χ^2 prob. ≥ 0.001	386	5.7	89.4
No e, μ	334	5.0	86.5
$0.05\ GeV/c \leq p_T^+ \leq 0.22\ GeV/c$	157	2.3	47.0
$c\tau \geq 0.1\ cm$	141	2.1	89.8

Table 5: The number of events passing the selection cuts for experimental data.

5 The K_S^0 sample

In the previous section samples of track pairs for the Monte Carlo signal and background as well as for the experimental data were obtained. The distributions of the invariant mass under the pion decay hypothesis for these samples are used to obtain the K_S^0 decay signal.

The invariant mass distributions for the candidates under the pion decay hypothesis before cuts are shown in Fig. 15. There is a difference between simulated and experimental data for low masses for reasons similar to those for the internal transverse momentum, as discussed in Section 4.10.

The invariant mass distributions for the candidates after cuts are shown in Fig. 16. The experimental data, on the left of the figure, clearly shows a mass peak between 0.46 GeV/c^2 and 0.54 GeV/c^2. For the normalization of the Monte Carlo background to the experimental data background, the region from 0.44 GeV/c^2 to 0.56 GeV/c^2 was excluded in order to ensure that no K_S^0-signal was used in the normalization. The resulting raw normalization factor for the MC background is 0.043. This can be compared to the normalization factor of 0.108 for "2+1+1"-events, as shown in Table 1. This discrepancy again points to differences in the track reconstruction efficiency, as discussed in Section 3.2.

In order to verify that the observed mass peak corresponds to K_S^0-particles, a gaussian fit is done on the peak to obtain the mean value and width. The width is a measure of the mass resolution of the detector for this measurement. The fit for the Monte Carlo sample is done only on signal events passing the selection cuts. For the experimental data, the background has to be taken into account as well. The procedure followed here was to directly fit the data to the Monte Carlo background, which was multiplied by a free scale factor, and a gaussian for the mass peak. The fits are shown in Fig. 17. The results for the mean of the gaussian for the Monte Carlo sample are $0.497 \pm 0.001\ GeV/c^2$ and for the sigma $0.018 \pm 0.001\ GeV/c^2$. For the experimental data, the

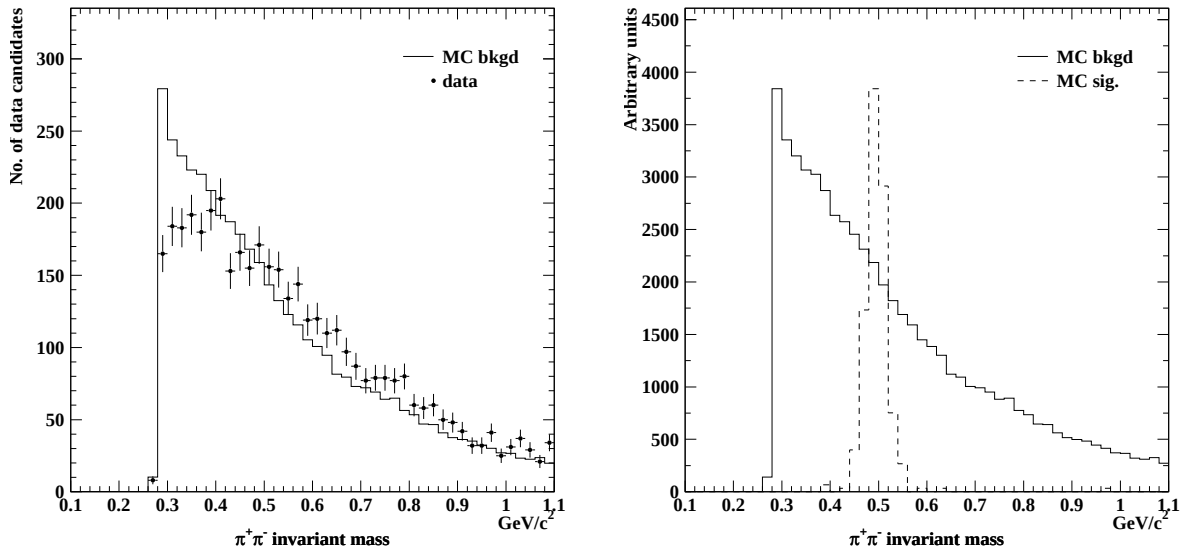

Figure 15: The invariant mass for all fully reconstructable track pairs under the pion decay hypothesis. The experimental data is compared to Monte Carlo background before cuts on the left. The distributions of the simulated signal and background for the combinations is shown on the right.

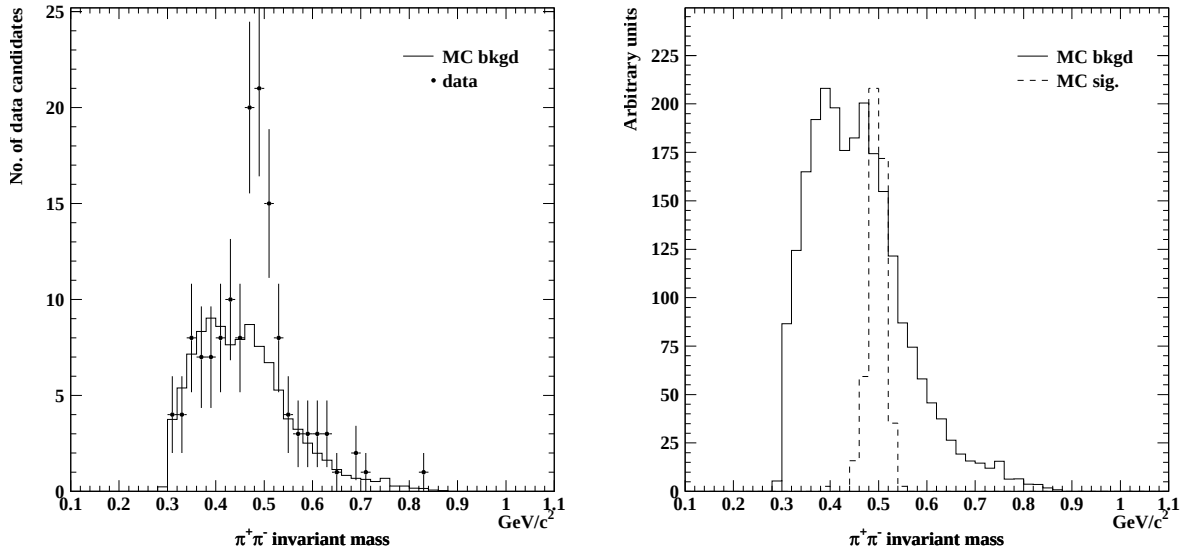

Figure 16: The invariant mass for all fully reconstructable track pairs under the pion decay hypothesis. The experimental data is compared to Monte Carlo background after cuts on the left. The normalization excludes the region from 0.44 GeV/c^2 to 0.56 GeV/c^2. The distributions of the simulated signal and background for surviving combinations is shown on the right.

values are 0.490 $\pm$ 0.006 GeV/c^2 and 0.021 $\pm$ 0.006 GeV/c^2, respectively. The scale-factor was found to be 0.042 $\pm$ 0.005, agreeing very well with the raw normalization factor for MC background of 0.043 found earlier in this section. The background was also estimated using fourth-order polynomial and spline functions, which produced nearly identical results to the one already quoted. One notes that the agreement between the MC and experimental data samples is good. The mass of the K_S^0 is quoted as 0.497672 $\pm$ 0.000031 GeV/c^2 in [6].

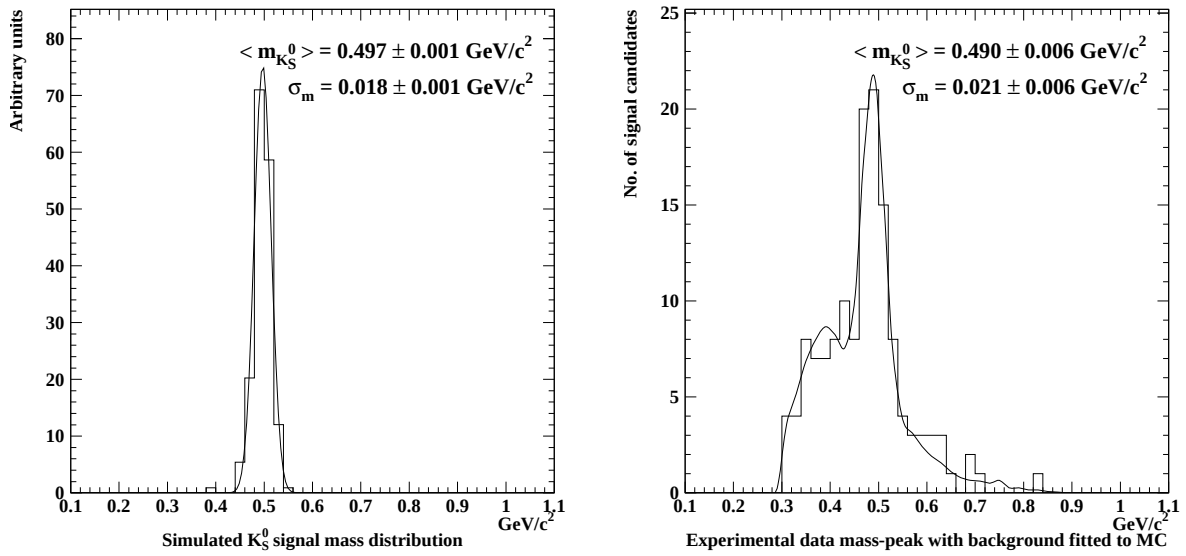

Figure 17: Gaussian fits to the peaks in the invariant mass distributions after cuts. On the left, the fit is done to the K_S^0 signal decays. On the right, the fit is done on the mass peak in the experimental data with an additional fit for the background.

To find the number of signal decays in the mass peak, the normalized Monte Carlo background sample is used to estimate the background in the experimental data in the mass peak region from 0.46 GeV/c^2 to 0.54 GeV/c^2. The mass peak contains a total of 64 decay candidates, while the estimation for the background gives 29 track pairs. We therefore expect there to be 35 K_S^0 decays. We calculate the statistical error using the error on the Monte Carlo sample and the error on the normalization to get 35 $\pm$ 9 K_S^0 decays in the experimental sample.

Using the 49.4% selection efficiency for signal events after cuts, shown in Table 3, and the estimated 35 signal decays in the experimental data, one finds that there should be 71 reconstructable K_S^0-particles before cuts in the experimental data sample. Taking into account the statistical errors on the selection efficiency and the estimated number of signal decays, we get 71 $\pm$ 19 decays. This is in agreement with the prediction of 52 $\pm$ 3 K_S^0 decays in Section 3.2. It should be noted that tighter cuts, which also implies less statistics, improve this agreement.

Next, as a further check of the validity of the analysis, we show in Fig. 18 the Armenteros plots for the unnormalized Monte Carlo sample and the experimental data sample. The Armenteros plot

shows the internal transverse momentum of the positive decay candidate, p_T^+, against the longitudinal momentum asymmetry variable, $\alpha = \frac{p_L^+ - p_L^+}{p_L^+ + p_L^-}$, where p_L^+ and p_L^- are the internal longitudinal momenta of the positive and negative decay candidates, respectively. The plot on the left in Fig. 18 shows that the K_S^0-signal in the Monte Carlo sample is restricted to the kinematically allowed elliptical band, as expected. Lambda-particles passing the selection cuts are also shown. From the distribution of the background, it is clear that the background is overwhelmed by random combinations of tracks. These tracks originate mainly from the primary vertex and are therefore usually not the result of V^0 decays. In fact, further studies on the Monte Carlo sample show that the contamination from pair production and lambda decay is small. On the right, the Armenteros plot for the experimental data is shown. The mass peak region of $0.46\ GeV/c^2 \leq m_{\pi^+\pi^-} \leq 0.54\ GeV/c^2$ is shown separately to the region outside the mass peak. As can be seen, all the candidates within the mass peak fall in the elliptical band suggested by the Monte Carlo signal decays. Therefore the Armenteros plot has no better discriminating power to reject background than does the invariant mass plot and it is not used as a selection cut.

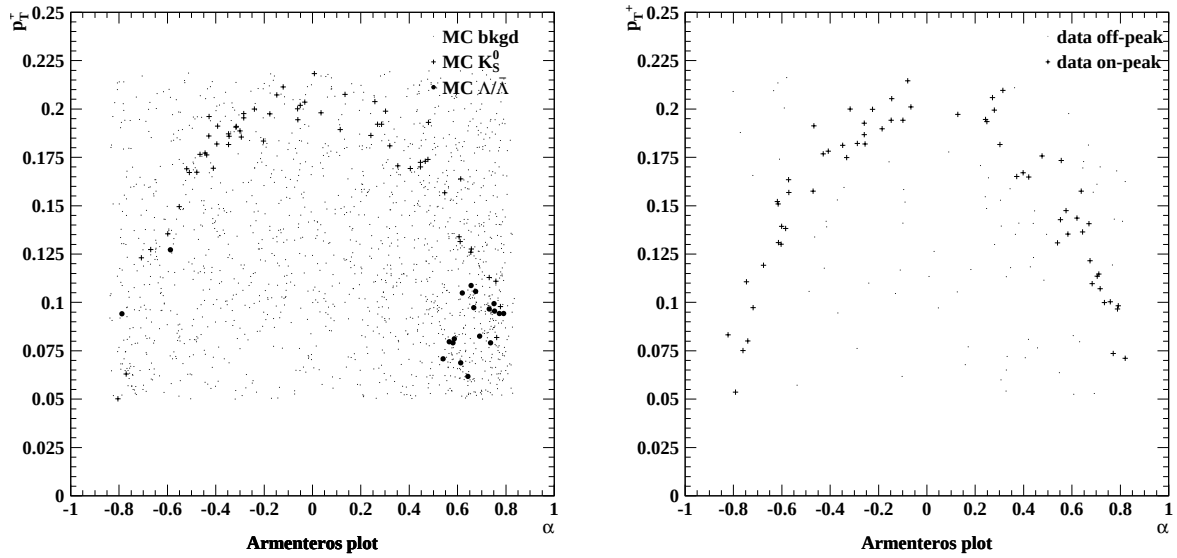

Figure 18: The Armenteros plots after all cuts. The results for the Monte Carlo sample are shown on the left, with the signal and background plotted separately. The distribution for the experimental data is shown on the right, with the mass peak region of $0.46\ GeV/c^2 \leq m_{\pi^+\pi^-} \leq 0.54\ GeV/c^2$ plotted separately to the rest of the mass region.

Finally, we discuss the normalization of the Monte Carlo signal sample to the Monte Carlo background sample. In fact, the two samples originate from a single Monte Carlo sample of neutrino interactions which included K_S^0 production. Normalizing both the Monte Carlo signal and background samples with the same weight of 0.043 that was previously found for the background gives the distribution for the $\pi^+\pi^-$ invariant mass as shown on the left of Fig. 19. As can be seen, the K_S^0 mass peak for the Monte Carlo simulation is not as prominent as for the experimental data. This again points to differences in the track reconstruction efficiency between the simulated and

experimental data samples with a possible contribution from the problem with Monte Carlo sample at the simulation level, as discussed in Section 3.2.

Due to the disagreement in the ratio of signal to background events between the Monte Carlo and experimental data samples, the signal and background in the Monte Carlo samples were normalized separately. To do this, the normalized background as obtained from the Monte Carlo sample, was first subtracted from the data, leaving the signal peak in the experimental data. Then the signal decays of the Monte Carlo sample which passed the selection cuts were normalized to the signal peak in the data. The raw normalization factor for the Monte Carlo signal sample using this method was 0.213, compared to 0.043 obtained for the background. Combining the resulting signal and background samples give the corrected Monte Carlo sample, shown on the right in Fig. 19. It should be pointed out that, as discussed before, tighter cuts improve the agreement between MC and data, resulting in normalization factors for the Monte Carlo background and signal which are closer to each other.

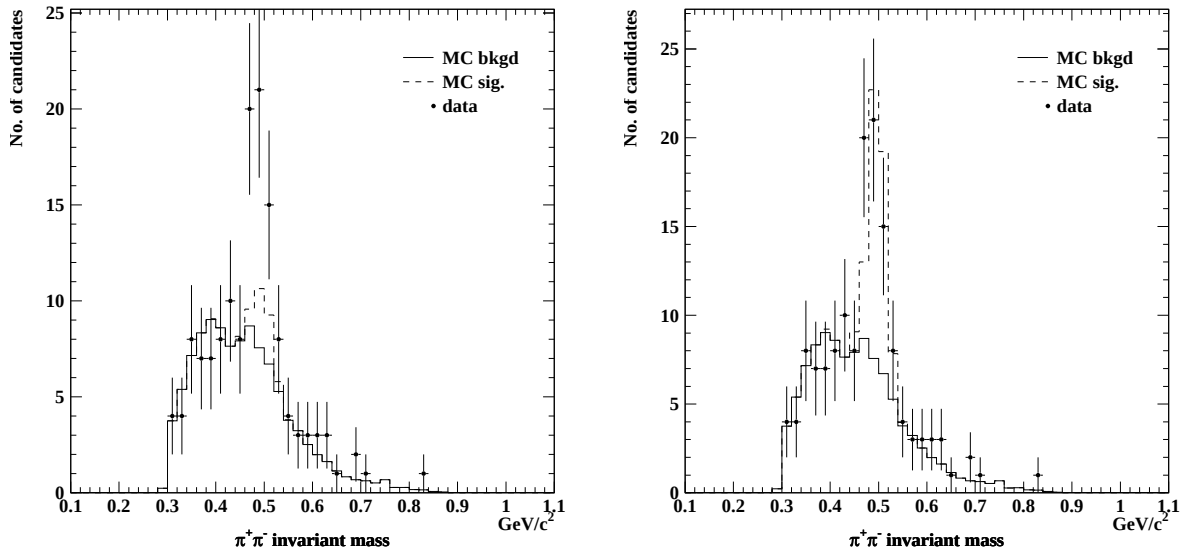

Figure 19: The invariant mass for all fully reconstructable track pairs under the pion decay hypothesis after cuts. The experimental data is compared to Monte Carlo samples with and without signal. The solid line represents the background, for which the raw normalization factor is 0.043. The dashed line shows the signal in addition to the background. On the left, the raw normalization factor of the Monte Carlo signal is 0.043, while on the right it is 0.213.

6 Vertex resolutions

In this section we discuss the various vertex resolutions of the NOMAD-STAR detector. As the Monte Carlo simulation is used for many of these measurements, our first aim is to show that the

Monte Carlo accurately simulates quantities related to the vertex resolutions. Once this is established, the simulation, together with the experimental data, can be used to obtain the required quantities. The results are obtained only for the y- and z-positions as STAR can only measure in these two directions. These two directions are always treated separately.

6.1 Primary vertex resolution

Initially the primary vertex is examined and the events are required to be of the "2+1+1"-configuration, i.e. a reconstructed primary vertex, composed of a minimum of two tracks, and in addition with at least one positive and one negative free track. The uncertainty in the reconstructed vertex position is defined as the square root of the covariance matrix element of the position of the vertex as obtained from the vertex fit [5]. This is obtained for both the simulated data and experimental data. The results are shown in Fig. 20. There is good agreement, which gives us confidence in the validity of those results obtained from the Monte Carlo alone. The shape of the end of the distribution in the z-position uncertainty and the cut-off at 500 μm are a consequence of the initial value of the uncertainty used in the iterative Kalman filtering procedure being too optimistic for poorly reconstructed vertices. This results in the vertex fit not converging properly. The rise in the distribution towards the 500 μm cut-off is due to poorly reconstructed two-track primary vertices.

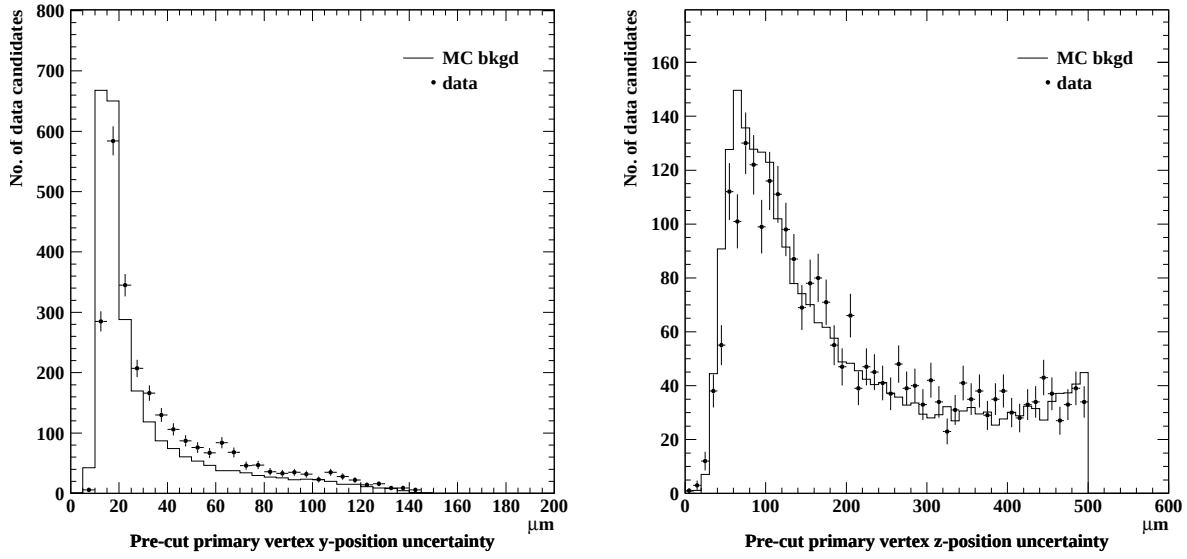

Figure 20: The uncertainty in reconstructed primary vertex position for "2+1+1"-events for Monte Carlo and experimental data before cuts. The results for the y-position are shown on the left and those for the z-position on the right.

The error in the reconstructed primary vertex is defined as the distance between the reconstructed and simulated positions for the primary vertex. This information can naturally only be obtained

from the simulated data. The distributions for the y- and z-positions are shown in Fig. 21 with the fit to a double gaussian distribution. We make the standard assumption that the principal error distribution is gaussian with an underlying background which is also gaussian. This background can be seen at the ends of the distributions (the "tails") in the figure and is due to tracks being poorly reconstructed as a result of multiple scattering. In fact, the total momentum and track multiplicity of these events is lower than for those events under the central peak. The fits indicate a resolution of 20.5 $\pm$ 0.3 μm for the y-position and 108 $\pm$ 3 μm for the z-position. The errors are statistical. This is in good agreement with the results for the vertex position uncertainty. The events at the ends of the distributions are due to low-momentum and low-opening angle primary vertices which have been poorly reconstructed.

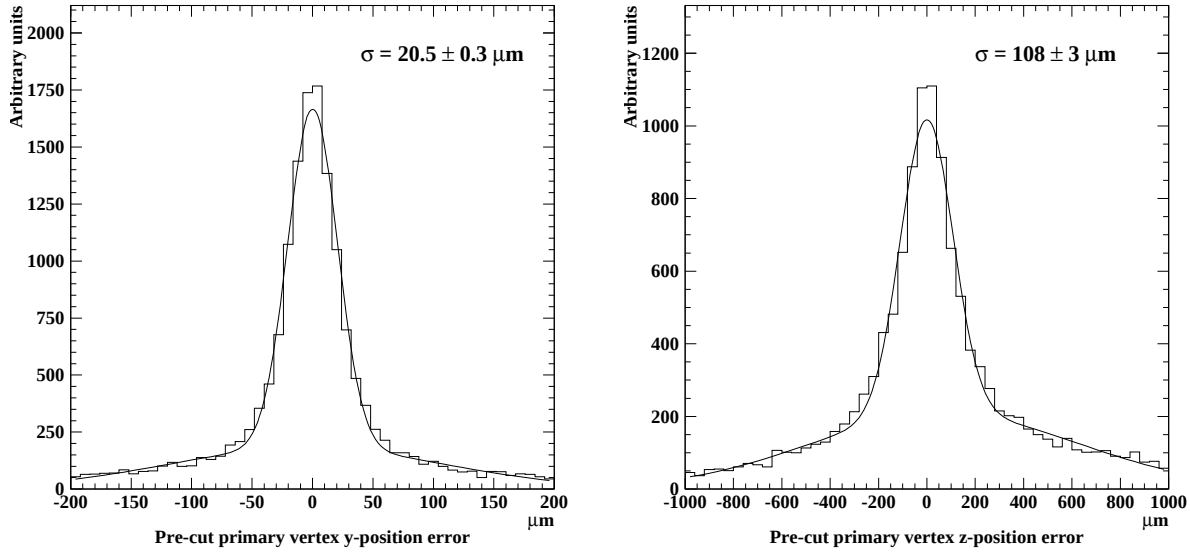

Figure 21: The error in reconstructed primary vertex position for "2+1+1"-events for Monte Carlo events before cuts. The fit is to a double gaussian distribution, with the y-position shown on the left and the z-position on the right.

6.2 Secondary vertex resolution

In this section we study the secondary vertex resolution. We first ascertain whether there is good agreement between the Monte Carlo simulation and the data by comparing the uncertainty distributions for fully reconstructable track pairs in a similar manner to what was done for the primary vertex. This is done before cuts as otherwise the number of events is too low for an accurate comparison. The signal decays which pass the cuts in the Monte Carlo simulation are used to obtain the uncertainty and error on the vertex position.

The uncertainties in the y- and z-positions for secondary vertex candidates before cuts are shown in Fig. 22. As for the primary vertex, the agreement between the y-position distributions is excellent.

The agreement between the z-position distributions is good. However, the slight discrepancy is again due to the difference in reconstruction efficiency of track pairs with a low opening angle, as discussed in Section 3.2. This, together with the excellent agreement in impact parameter, discussed in Section 4.4, gives us confidence in the results which are obtained from the Monte Carlo simulation alone. As for the case of the primary vertex, the cut-off at 500 μm in the z-position uncertainty is a consequence of the vertexing algorithm. The secondary vertex position uncertainty for Monte Carlo signal events is shown in Fig. 23 and is in good agreement with Fig. 22, indicating that the pre- and post-cut secondary vertex uncertainties are similar.

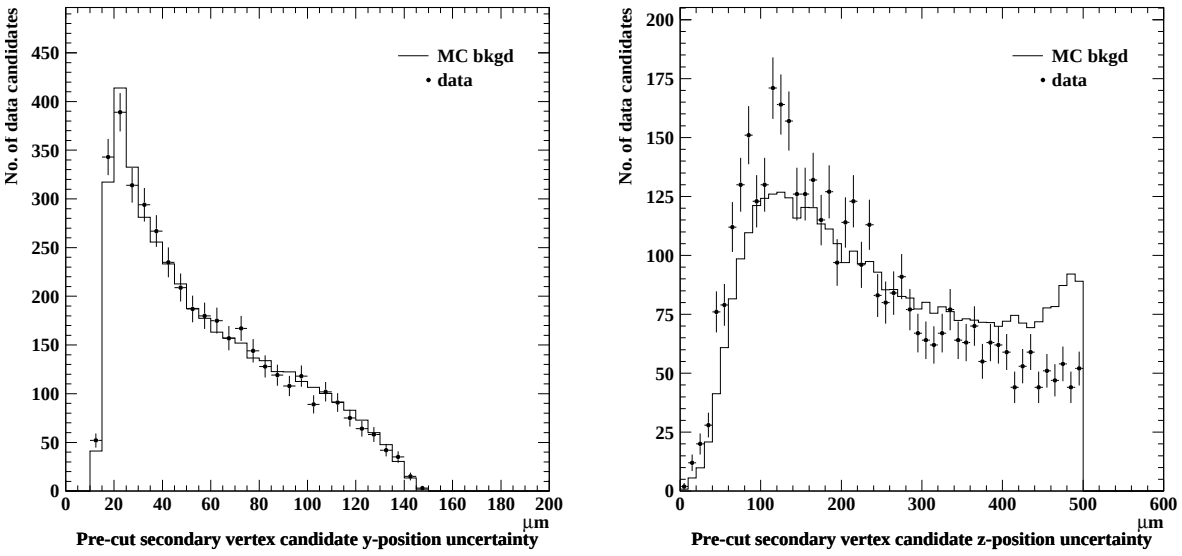

Figure 22: The uncertainty in position for reconstructed secondary vertex candidates before cuts. The results for the y-position are shown on the left and those for the z-position on the right.

The error on the secondary vertex position is shown in Fig. 24. The fit is to a double gaussian and indicates a y-position secondary vertex resolution of 19 ± 6 μm and a z-position resolution of 60 ± 10 μm. These values are slightly better than those obtained for the primary vertex. This is to be expected, as the correct reconstructed tracks for the secondary vertices, by virtue of the Monte Carlo simulation, are selected. This implies that the tracks have to be identifiable and therefore be well reconstructed. Furthermore, the large opening angle gives a better z-resolution. On the other hand, when building primary vertices, the simulated tracks are not identified using the Monte Carlo information and therefore some poorly reconstructed tracks could also be used, decreasing the resolution in these cases. It should be noted that for all the error resolutions shown, a significant number of entries are outside the central gaussian fit. This is true in particular for the z-resolutions. However, this situation is expected to improve for tau and charm decays as the decay particles have a higher average momentum and are therefore easier to reconstruct correctly.

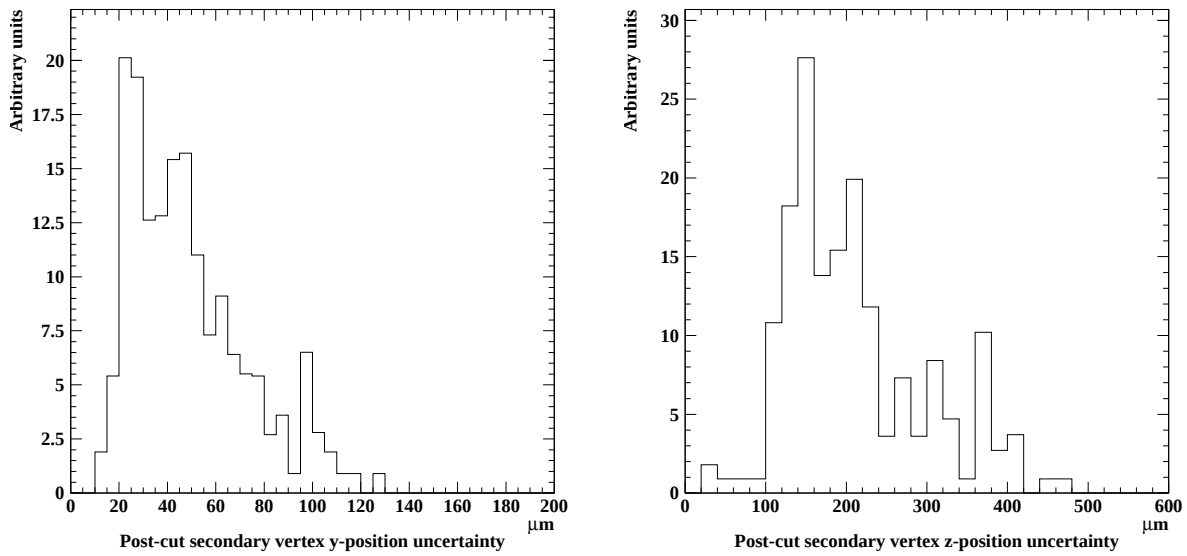

Figure 23: The uncertainty in position after cuts for reconstructed secondary vertices identified as signal from the Monte Carlo simulation. The results for the y-position are shown on the left and those for the z-position on the right.

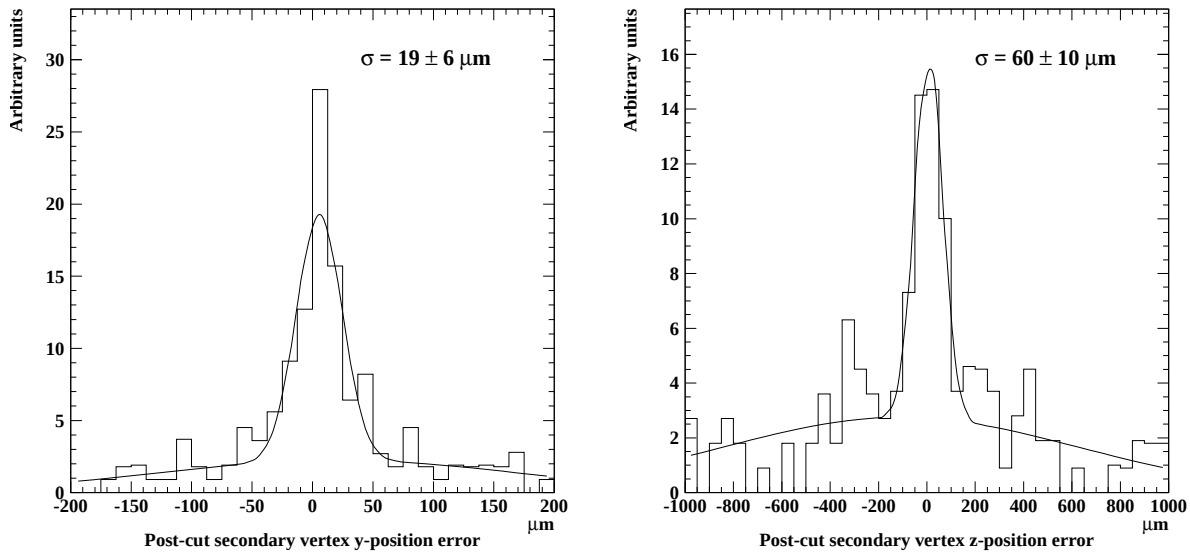

Figure 24: The error in position after cuts for reconstructed secondary vertices identified as signal from the Monte Carlo simulation. The fit is to a double gaussian distribution with the y-position shown on the left and the z-position on the right.

6.3 Double vertex resolution

The double vertex resolution is defined as the square-root of the variance of the distribution of the difference in separation between the primary and secondary vertex positions for the simulated vertices and for the reconstructed vertices. It is therefore a measure of the error in determining the separation between the primary and secondary vertices and can only be obtained using the simulated data. We present two different methods to do this. Firstly, the signal events which pass the cuts in the Monte Carlo simulation are used. Secondly, a method of subtracting the background from the mass peak using neighbouring regions is shown.

The distribution for the double vertex resolution obtained using the Monte Carlo simulated candidates which pass the cuts, as required in the first method, is shown in Fig. 25. A fit to a double gaussian distribution gives a y-resolution of 18 $\pm$ 4 μm and a z-resolution of 280 $\pm$ 40 μm. As already noted when discussing the primary vertex resolution, the events at the ends of the distributions are due to poorly reconstructed low-momentum or low-opening angle primary vertices. It should be further noted that the fit for the z-resolution is not ideal.

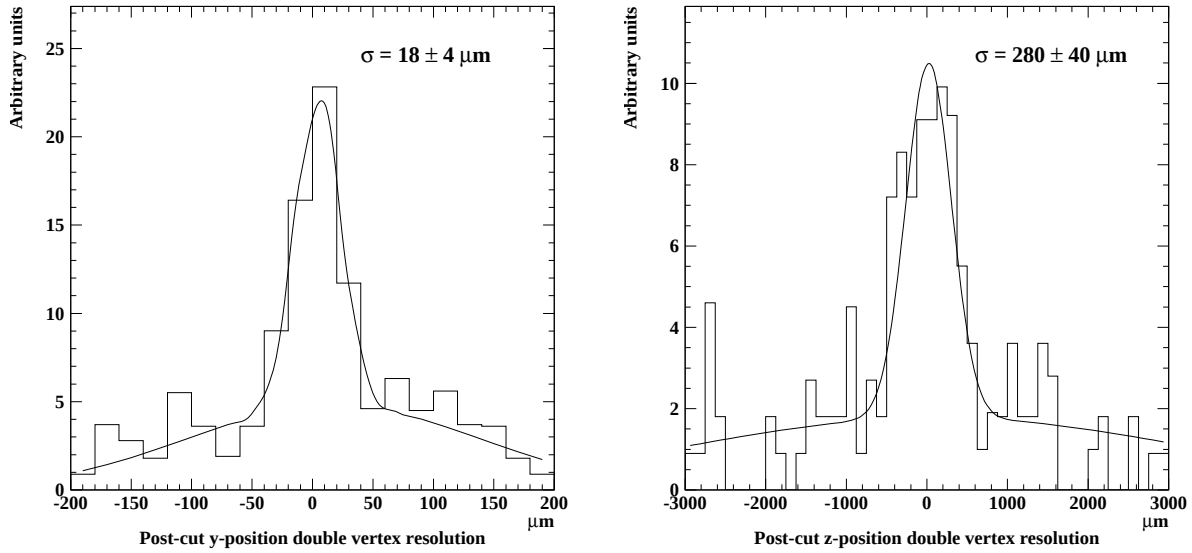

Figure 25: The double vertex resolution after cuts for the signal decays obtained from the Monte Carlo simulation. The fit is to a double gaussian distribution with the y-position shown on the left and the z-position on the right.

In the second method, the double vertex resolution is obtained by subtracting the contribution due to the background from the mass peak. This method uses the normalization of signal to background events, as obtained previously from the experimental data. Here, the Monte Carlo background events are normalized to the signal events. As found in Section 5, the normalization factors Monte Carlo signal and Monte Carlo background, are 0.213 and 0.043, respectively, as obtained in Section 5. Therefore the relative weight of Monte Carlo background events to signal events is 0.202.

As a first step, the distribution for the error in the vertex separation is obtained under the mass peak, which is defined as the region from 0.46 GeV/c^2 to 0.54 GeV/c^2. This mass peak naturally contains both signal and background track pairs. For signal pairs the error is obtained in the straightforward manner using the definition described earlier. However, it is not possible to calculate the vertex separation error for background pairs using the definition as a true secondary vertex does not exist in that case. In these instances it is assumed that the tracks composing the pair originate from the primary vertex and the position of the primary vertex is also taken as the position of the secondary vertex. Thus the double vertex error is the full reconstructed distance between the primary vertex and secondary vertex candidate. The double vertex error distributions for the on-peak mass regions from 0.46 GeV/c^2 to 0.54 GeV/c^2 are shown in Fig. 26.

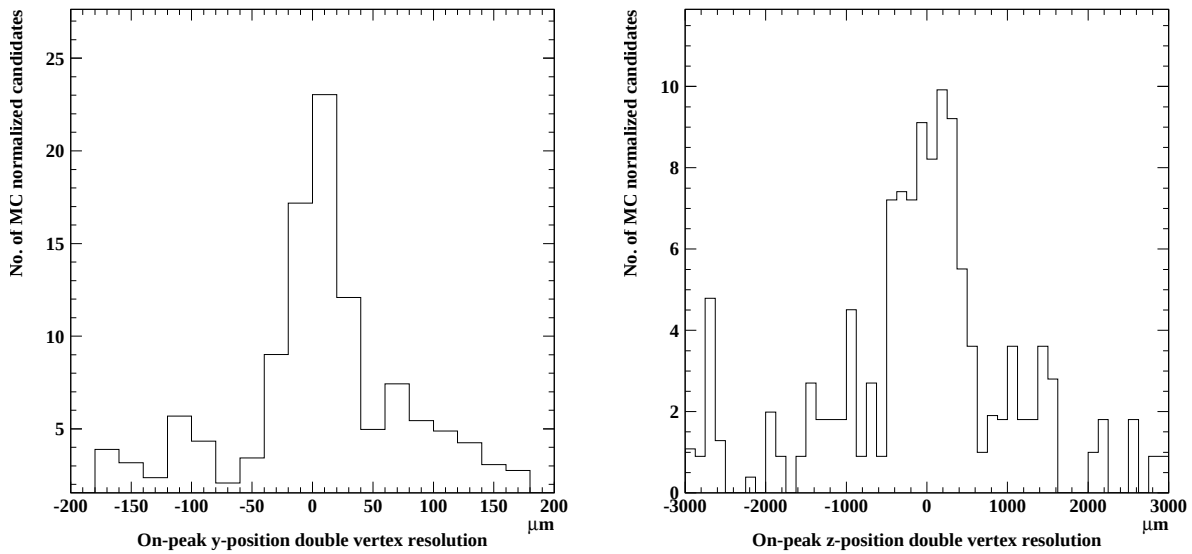

Figure 26: The double vertex error distributions in the Monte Carlo simulation for the mass peak region, defined as the region from 0.46 GeV/c^2 to 0.54 GeV/c^2. The distribution for the y-position is shown on the left and for the z-position on the right.

In order to subtract the background in the mass peak, the contribution due to the background is estimated using the two mass regions from 0.42 GeV/c^2 to 0.46 GeV/c^2 and from 0.54 GeV/c^2 to 0.58 GeV/c^2, which are next to the mass peak. In these off-peak regions the vertex separation error is calculated as before: in the case of stray signal, using the definition and in the case of background, using the full reconstructed distance between vertices. Next, the error distribution obtained from the two off-peak mass regions is normalized to the number of background candidates in the mass peak using the number of events. These normalized off-peak double vertex error distributions are shown in Fig. 27.

The normalized distribution of errors is then subtracted from the full distribution under the mass peak. This gives the final double vertex error distribution. A fit is done to obtain the double

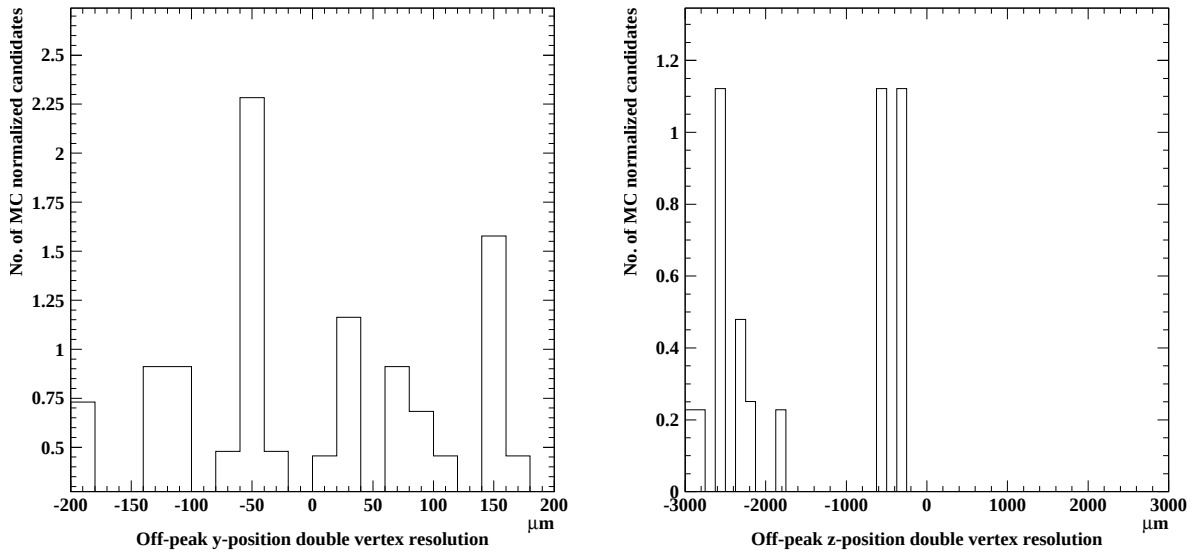

Figure 27: The double vertex error distributions for the off-mass peak regions from 0.42 GeV/c^2 to 0.46 GeV/c^2 and 0.54 GeV/c^2 to 0.58 GeV/c^2. They have been normalized such that the number of events in the off-peak regions is the same as the number of background events in the on-peak region. The distribution for the y-position is shown on the left and for the z-position on the right.

vertex resolution. As before, the central peak is assumed gaussian. However, no gaussian assumption is made on the background double vertex error due to the way it is calculated and instead a second-order polynomial is used. The fits result in a y-resolution of 19 ± 4 μm and a z-resolution of 310 ± 30 μm. The results are shown in Fig. 28. These are in agreement with the results of 18 ± 4 μm for the y-position and 280 ± 40 μm for the z-position obtained using the pure Monte Carlo simulated signal sample.

7 Conclusion

This study shows that the NOMAD-STAR detector is capable of detecting K^0_S-particles through their decay to charged pions. The reconstruction efficiency of reconstructable K^0_S-particles in the Monte Carlo sample was found to be 13.0 %. Of these, 49.4 % passed the selection cuts. The 1998 experimental data sample consisted of 10942 neutrino interactions with a STAR-reconstructed primary vertex. This was used to extract 64 K^0_S candidate particles with an estimated background of 29. This leaves, considering the statistical error, 35 ± 9 K^0_S particles after selection cuts. The mass was measured to be 0.490 ± 0.006 GeV/c^2, agreeing well with the world average value of 0.498 GeV/c^2, while the mass resolution for this measurement was found to be 0.021 ± 0.006 GeV/c^2.

In general, the experimental data was in good agreement with the Monte Carlo simulated data,

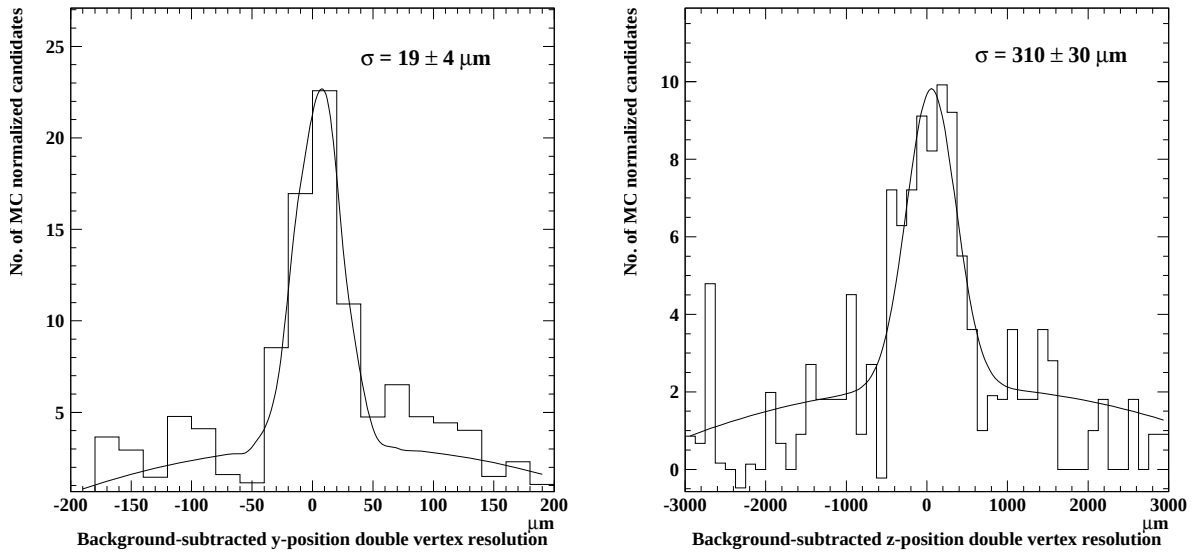

Figure 28: The double vertex resolution after subtraction of background from the mass peak, defined as the region from 0.46 GeV/c^2 to 0.54 GeV/c^2. The fit is primarily to a gaussian distribution, with a second-order polynomial used for the background. The distribution for the y-position is shown on the left and that of the z-position on the right.

although there were some differences in track reconstruction efficiency and two-track resolution for low opening angles. In particular, the vertex-related parameters were in good agreement, allowing the Monte Carlo sample to be used to determine the vertex resolutions. The primary vertex resolution (for events requiring at least two tracks in the primary vertex as well as at least one free positive and one free negative track), was found to be 20.5 $\pm$ 0.3 μm for the y-position and 108 $\pm$ 3 μm for the z-position. The resolution for K^0_S decay vertices passing the selection cuts was found to be 19 $\pm$ 6 μm and 60 $\pm$ 10 μm for the y- and z-positions, respectively. The double vertex resolution for these events was found to be 18 $\pm$ 4 μm and 280 $\pm$ 40 μm for the y- and z-positions, respectively. An alternative method to calculate the double vertex resolution, which used both signal and background events to obtain the double vertex error and in which the estimated effect of the background was then subtracted, yielded a resolution of 19 $\pm$ 4 μm and 310 $\pm$ 30 μm for the y- and z-positions, respectively.

Acknowledgements

I would like to thank L. Camilleri, M. Ellis, L. Linssen and P. Soler for the considerable time, effort, suggestions and comments they have contributed to this analysis. Furthermore, I am indebted to all others contributing to STAR through their time and effort. In addition to the people already mentioned, these would include at least A. Cervera-Villanueva, E. do Couto e Silva, D. Ferrère, J.J. Gomez-Cadenas, M. Gouanère, J.A. Hernando, V.E. Kuznetsov, Ö. Runolfsson,

G. Baricchello, D.C. Daniels, L. Dumps, C. Gößling, S. Geppert Soulie, W. Huta, J.M. Jimènez, B. Lisowski, J. Long, A. Lupi, K. Mühlemann, J. Mulon, B. Schmidt, D. Steele, M. Stipčević, M. Veltri, G. Vidal-Sitjes and D. Voillat. Finally, I thank the NOMAD institutions for their encouragement and support.

References

[1] *The NOMAD Experiment at the CERN SPS*, J. Altegoer *et al.*, NOMAD Collaboration, Nuclear Instruments and Methods Phys. Res. A 404 (1998) 96-128.

[2] *A B_4C-Silicon Target for the Detection of Neutrino Interactions*, G. Baricchello *et al.*, Nuclear Instruments and Methods Phys. Res. A 419 (1998) 1-15.

[3] *A Study of Charm Production by Neutrinos in the NOMAD-STAR Detector*, M. Ellis, Doctoral Thesis, University of Sydney (2001).

[4] *Performance of Long Modules of Silicon Microstrip Detectors*, G. Baricchello *et al.*, Nuclear Instruments and Methods Phys. Res. A 413 (1998) 17-30.

[5] *Kalman Filter Tracking and Vertexing in a Silicon Detector for Neutrino Physics*, A. Cervera-Villanueva *et al.*. Submitted to Nuclear Instruments and Methods Phys. Res. A.

[6] *Review of Particle Physics*, Particle Data Group. Eur. Phys. J. C 15 (2000) 1-878.

[7] *GEANT-Detector Description and Simulation Tool.* CERN Program Library Long Writeup W5013 (1994).